

Large Fermi energy modulation in graphene transistors with high-pressure O₂-annealed Y₂O₃ topgate insulators

Kaoru Kanayama, *Kosuke Nagashio, Tomonori Nishimura, and Akira Toriumi

Department of Materials Engineering, The University of Tokyo 7-3-1 Hongo, Bunkyo-ku, Tokyo, 113-8656, Japan

*Email: nagashio@material.t.u-tokyo.ac.jp

We demonstrate a considerable suppression of the low-field leakage through a Y₂O₃ topgate insulator on graphene by applying high-pressure O₂ at 100 atm during post-deposition annealing (HP-PDA). Consequently, the quantum capacitance measurement for the monolayer graphene reveals the largest Fermi energy modulation ($E_F = \sim 0.52$ eV, i.e., the carrier density of $\sim 2 \times 10^{13}$ cm⁻²) in the solid-state topgate insulators reported so far. HP-PDA is the robust method to improve the electrical quality of high- k insulators on graphene.

The deposition of ultrathin and reliable high- k dielectrics on graphene is required to realize the high transconductance in graphene field-effect transistors (FETs). Generally, two kinds of deposition methods are used: one is physical vapor deposition¹⁻⁴ (PVD) with low particle energies to avoid the defect introduction in graphene,⁵ the other is atomic layer deposition (ALD) with buffer layers⁶⁻⁸ to overcome the chemically inert surface of graphene. Recently, graphene FETs have been reported with ALD Al₂O₃ topgate insulators as thin as 2.6 nm.⁹

Insulators fabricated by PVD and ALD, however, suffer from the dielectric breakdown at the voltage much lower than the complete breakdown voltage due to the fragility of dielectrics accumulated by the low-field leakage during the iterative measurements. Typical electrical field for this low-field dielectric breakdown is ~ 0.2 V/nm. This is a critical issue for the reliability of the topgate insulators. A common limitation for the insulators on graphene fabricated by both PVD and ALD is the lack of a robust methodology for post-deposition annealing (PDA) in an O₂ atmosphere. Although PDA at a high temperature (e.g., ~ 500 °C) is known to improve the electrical quality of the insulator considerably,¹⁰ it introduces many defects in graphene by oxidation.¹¹

Here, from a thermodynamic viewpoint,¹² let's consider the Gibbs free energy change ($\Delta G = \Delta G^\circ - RT \ln P_{O_2}$) for the oxidation reaction of $M + O_2 = MO_2$, where ΔG° is the standard Gibbs free energy change for the oxidation reaction, R is gas constant, P_{O_2} is the oxygen partial pressure and M is the metal. ΔG should be

negative to facilitate the oxidation. The first term for ΔG can be used for material selection. An appropriate rare-earth element for use in high- k insulators should be highly susceptible to oxidation. **Figure 1(a)** shows ΔG° of rare-earth, transition and representative elements at 300 °C calculated using a thermodynamic database.¹³ The ΔG° for yttrium is negatively largest among all of the metal oxides, even smaller than that of carbon. Therefore, Y₂O₃ can be obtained at relatively low oxidation temperatures and is thermodynamically stable on graphene. The band gap for Y₂O₃ is ~ 5.5 eV, which is almost identical to that of h-BN.¹⁴ The dielectric constant of Y₂O₃ is ~ 12 ,¹⁵ while it is $\sim 3-4$ for h-BN.¹⁶ The second term for ΔG is the process condition, which is derived from the oxygen potential. ΔG should be further decreased to reduce the defects in the insulator such as oxygen vacancy. This can be achieved by increasing P_{O_2} during PDA without elevating the annealing temperature.

The strategy for fabricating high-quality high- k insulators on graphene is the deposition of Y₂O₃ on graphene by PVD with low particle energy and a subsequent high-pressure PDA (HP-PDA) process carried out in a 100 % O₂ atmosphere at ~ 100 atm and 300 °C. In this study, we demonstrate drastic suppression of the low-field leakage current through a Y₂O₃ topgate using HP-PDA. The improved electrical quality of the insulators on the monolayer graphene is realized by the large modulation of Fermi energy (E_F) in the quantum capacitance (C_Q) measurements as well as the high transistor performance in the electrical transport measurements.

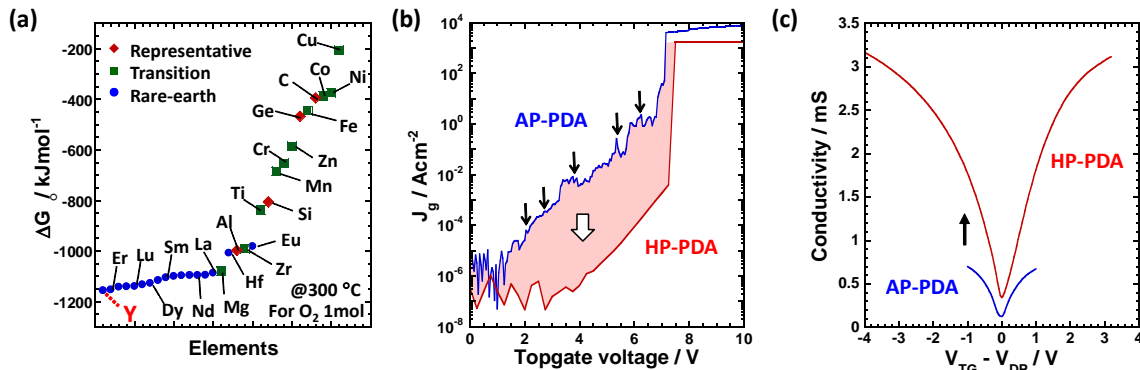


FIG 1. (a) ΔG° of rare-earth, transition and representative elements at 300 °C, calculated using a thermodynamic database. The ΔG° value for 1 mol of O₂ is shown, for mainly two kinds of oxidation reactions, $M + O_2 = MO_2$ and $4/3M + O_2 = 2/3M_2O_3$. For the rare-earth elements, only several important elements are shown due to the lack of space. (b) Leakage current density through the Y₂O₃ topgate insulators fabricated by HP-PDA and AP-PDA. (c) σ as a function of $V_{TG} - V_{DP}$ for the graphene FETs fabricated by HP-PDA and AP-PDA.

We fabricated monolayer graphene backgated FETs containing source and drain electrodes (Ni(~ 10 nm)/Au(~ 50 nm)) on ~ 90 nm $\text{SiO}_2/\text{n}^+\text{-Si}$ substrates by the mechanical exfoliation of Kish graphite. Y_2O_3 was then deposited over the entire surface area of the wafer by the thermal evaporation of $\sim 2 - 2.5$ mg of Y metal in the O_2 atmosphere, where the P_{O_2} was adjusted to 10^{-1} Pa.⁴ The thickness was roughly controlled at $\sim 5 - 7$ nm by selecting the initial mass of the Y metal. Next, the samples were placed in a high-pressure annealing system made of Inconel 625 alloy (supplementary material¹⁷), which is generally used for supercritical fluid experiments. The HP-PDA process was carried out in a 100 % O_2 atmosphere at ~ 100 atm at 300 °C for 20 min. Finally, the topgate electrode (Ni/Au) was patterned, followed by annealing at 300 °C for 30 s under 0.1% O_2 gas flow. For comparison with the HP-PDA process, atmospheric-pressure PDA (AP-PDA) was also carried out in a 100 % O_2 atmosphere at 1 atm at 200 °C for 10 min, which is the same condition used in the previous work.⁴ The lack of a Raman D band measured through Y_2O_3 indicated that no defects were introduced into graphene by the HP-PDA process.¹⁷

Figure 1(b) compares the leakage current density (J_g) through Y_2O_3 between the source and the topgate fabricated by HP-PDA and AP-PDA. There are many small spikes in J_g for AP-PDA, as shown by black arrows, suggesting that defect states exist within the band gap. After HP-PDA, the drastic suppression of the low field leakage current is clearly observed. Especially, small spikes completely disappear. On the other hand, the complete breakdown voltage does not change much. **Figure 1(c)** compares the conductivity (σ) as a function of the topgate voltage (V_{TG}) on the basis of the Dirac point voltage (V_{DP}) for the graphene FETs fabricated by HP-PDA and AP-PDA. It is evident that HP-PDA is effective for the transconductance improvement.

Figure 2(a) shows the resistivity (ρ) as a function of V_{TG} for different backgate voltages (V_{BG}) at 20 K. The

topgate leakage current of $\sim 10^{-12}$ A, as shown in the inset of **Fig. 2(a)**, is seven orders of magnitude lower than the source-drain current (I_{SD}) of $\sim 10^{-5}$ A. The topgate voltage can be swept over a wide range of ± 4 V; therefore, the V_{BG} is widely swept by ± 60 V after the leakage current and complete breakdown voltage for the backgate SiO_2 insulator with ~ 90 nm in thickness are confirmed.

To qualitatively compare the electrical quality of the Y_2O_3 insulator with previous reports, we judged the insulator not from the relationship between J_g and the equivalent oxide thickness (EOT) but rather from the maximum E_F modulation estimated by the C_Q measurement. **Figure 3(a)** shows the total capacitance (C_{total}) values between the source and topgate electrodes as a function of V_{TG} for varying V_{BG} at 20 K. The C_{total} was strongly dependent on the V_{TG} . For channel materials with low density of states (DOS), such as graphene, the C_{total} can be described by $1/C_{\text{total}} = 1/C_{\text{ox}} + 1/C_Q$, where C_{ox} is the geometric capacitance and $C_Q = e^2 \text{DOS}$.¹⁸ This is because the increase in the energy to induce carriers in the channels with low DOS is large and is introduced as a voltage drop in the equivalent circuit. The simplified equivalent circuit, in which V_{DP} is held at $V_{\text{TG}} = 0$ V by adjusting the V_{BG} , is shown in **Fig. 3(b)**. The hysteresis in bidirectional C - V measurements is negligible for ± 4 V sweep of V_{TG} ,¹⁹ as shown in **Fig. 3(c)**, suggesting the good quality of the Y_2O_3 insulator. **Figure 3(d)** compares the C_{Total} as a function of $V_{\text{TG}} - V_{\text{DP}}$ for the graphene FETs fabricated by HP-PDA and AP-PDA.⁴ A considerable increase in the C_{Total} was clearly observed, indicating an increase in $C_{\text{Y}_2\text{O}_3}$ by HP-PDA. This is consistent with the increase in the transconductance, as shown in **Fig. 1(c)**.

For qualitative estimation of the $C_{\text{Y}_2\text{O}_3}$, the V_{DP} for the topgate sweep was plotted as a function of the V_{BG} , as shown in **Fig. 2(b)**. The DP shift of the I - V data is almost consistent with the shift of the C - V data. The average slopes of the I - V and C - V data for HP-PDA, which correspond to the capacitive coupling of $C_{\text{SiO}_2}/C_{\text{Y}_2\text{O}_3}$, are more gradual than those observed for AP-PDA. Using $C_{\text{SiO}_2} = 0.038 \mu\text{Fcm}^{-2}$ for a 90 nm thickness of SiO_2 , the

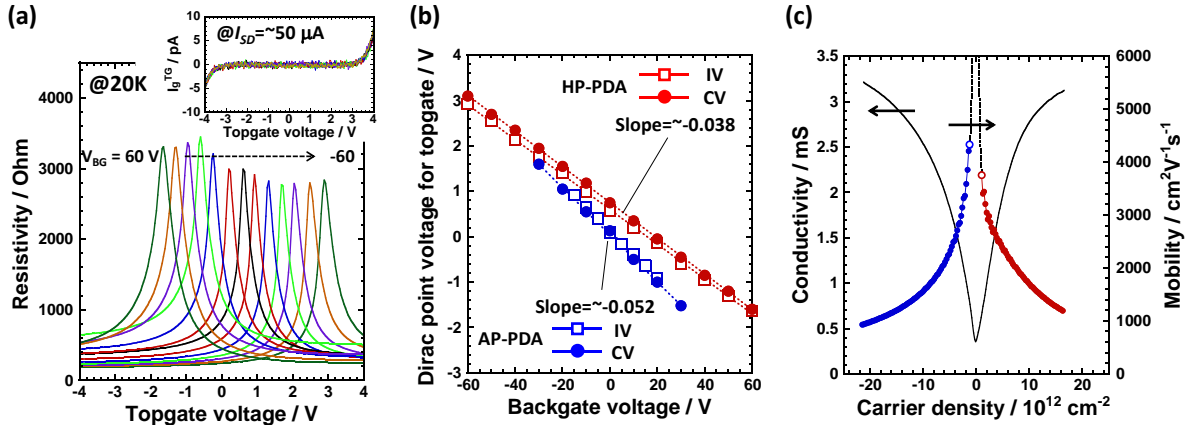


FIG 2. (a) ρ as a function of V_{TG} for different V_{BG} at 20 K. The inset shows the topgate leakage current for $I_d \sim 50 \mu\text{A}$. (b) V_{DP} for the V_{TG} sweep as a function of the V_{BG} . The red solid circles and red solid boxes indicate the DPs obtained by I - V and C - V measurements for HP-PDA in Fig. 2(a) and Fig. 3(a), respectively. The blue data are adapted from a previous work.⁴ The slopes are determined by linear fitting. (c) σ and μ as a function of n . The mobility for $n < 1 \times 10^{12} \text{cm}^{-2}$ is not valid due to n^* .

$C_{Y_2O_3}$ for HP-PDA is calculated to be $0.95 \mu\text{Fcm}^{-2}$, which is indeed improved from $C_{Y_2O_3} = 0.76 \mu\text{Fcm}^{-2}$ for AP-PDA.⁴ In the equivalent circuit shown in **Fig. 3(b)**, there is only one fitting parameter for the parasitic capacitance (C_{para}), as the C_Q can be calculated by the theoretical relation of $C_Q = 2e^2 E_F / \pi (v_F \hbar)^2$, where v_F is the Fermi velocity ($1 \times 10^8 \text{ cm/s}$) and \hbar is Planck's constant. The experimental data are fit by solid lines in **Fig. 3(d)** using $C_{\text{para}} = 0.10 \mu\text{Fcm}^{-2}$ for HP-PDA and $C_{\text{para}} = 0.19 \mu\text{Fcm}^{-2}$ for AP-PDA. The C_Q is obtained simply from $C_Q = C_{Y_2O_3} C'_{\text{total}} / (C_{Y_2O_3} - C'_{\text{total}})$, where $C'_{\text{total}} = C_{\text{total}} - C_{\text{para}}$. **Figure 3(e)** shows the C_Q as a function of E_F in the graphene FETs fabricated by HP-PDA. The C_Q for AP-PDA is shown for comparison. The charging energy required to induce carriers in the graphene is denoted by E_F , which is expressed as $E_F = eV_{\text{ch}}$. V_{ch} can be expressed by the equation for a series combination of capacitors according to $V_{\text{ch}} = V'_{\text{TG}} - \int_0^{V'_{\text{TG}}} C'_{\text{Total}} / C_{Y_2O_3} dV'_{\text{TG}}$, where V'_{TG} is defined as $V'_{\text{TG}} = V_{\text{TG}} - V_{\text{DP}}$. The deviation from the theoretical value near the DP is due to residual carriers that are externally induced by the charged impurities.^{2,4,20} The residual carrier density (n^*), as shown by the arrow in **Fig. 3(e)**, is calculated as $3.6 \times 10^{11} \text{ cm}^{-2}$ using $E_F = \hbar v_F \sqrt{\pi n^*}$. The n^* values for HP-PDA and AP-PDA are almost the same, although there are device-to-device variations. The estimated C_Q value for HP-PDA is consistent with the theoretical dotted line for $E_F > \sim 0.15 \text{ eV}$, suggesting that HP-PDA has no influence on the band structure of graphene. **Table 1** compares the maximum E_F values reported in the literature. The data obtained by the ion gating are also included. Although there are many reports on electron transport in topgated graphene FETs, the literature for C_Q measurements is selected because relatively high-quality and thin topgate

insulators are required. The largest E_F values (0.52 eV) for solid-state topgate insulators are achieved by HP-PDA.

Now, let's move back to the transport measurement to extract the carrier mobility (μ). The carrier density (n) cannot be evaluated by a simple parallel plate capacitor model for geometric capacitance, because of the significant contribution of the C_Q . Here, n is evaluated by the integral of the differential capacitance C'_{total} ,²¹ i.e., $n = \frac{1}{e} \int_0^{V'_{\text{TG}}} C'_{\text{Total}} dV'_{\text{TG}}$. Then, μ is calculated from $\mu = \sigma / en$. **Figure 2(c)** shows σ and μ as a function of n . A large n of $\sim 2 \times 10^{13} \text{ cm}^{-2}$ is reached because of the improved $C_{Y_2O_3}$ and the large voltage applied only to the Y_2O_3 insulator ($V_{\text{TG}} - V_{\text{ch}} = \sim 3.6 \text{ V}$). Although n is evaluated by the integral of C'_{total} , it still includes the contribution from n^* near the DP. Therefore, μ for $n < 1 \times 10^{12} \text{ cm}^{-2}$ is neglected. The high μ of $\sim 4,100 \text{ cm}^2 \text{V}^{-1} \text{ s}^{-1}$ is much improved from the previous AP-PDA device,⁴ even though the contribution of the contact resistance is included in this device.

Next, we discuss the physical and chemical origins for the drastic improvement of the Y_2O_3 insulator fabricated by HP-PDA. The X-ray photoelectron spectra were measured for the Y_2O_3 films on highly oriented pyrolytic graphite (HOPG) with HP-PDA and AP-PDA.¹⁷ The peaks for C_{1s} , Y_{3d} and O_{1s} are almost the same for HP-PDA and AP-PDA. Therefore, the oxidation state of the Y element is not drastically affected by HP-PDA. Moreover, the average surface roughness of the Y_2O_3 film on the HOPG with HP-PDA and AP-PDA are $\sim 0.36 \text{ nm}$ and $\sim 0.34 \text{ nm}$, respectively, again suggesting no clear difference.

The main difference is evident in the cross-sectional transmission electron microscope (TEM) images of the

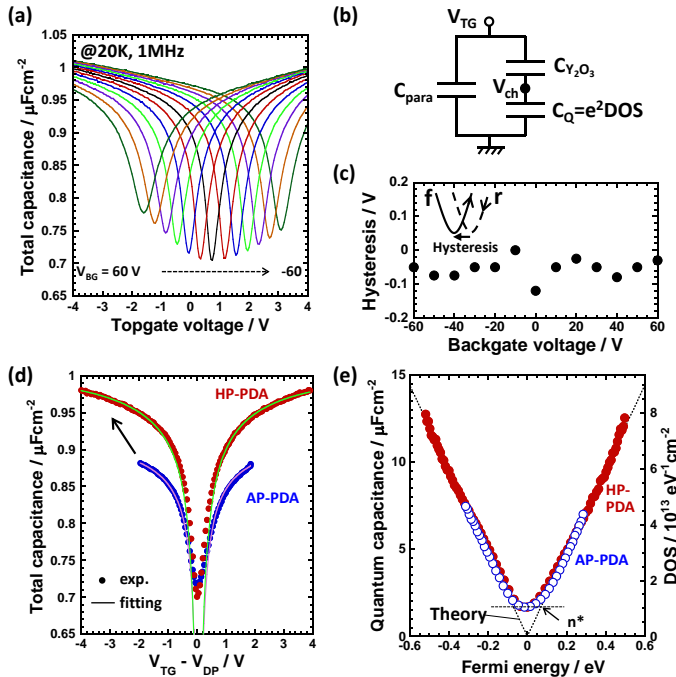


FIG 3. (a) C_{Total} as a function of V_{TG} for the graphene FET device at 20 K at a frequency of 1 MHz. (b) The equivalent circuit simplified for the topgate graphene FET device, in which V_{DP} is placed at $V_{\text{TG}} = 0 \text{ V}$ by adjusting the V_{BG} . (c) Hysteresis detected in the sweeping range of $\Delta V_{\text{TG}} = \pm 4 \text{ V}$ for different V_{BG} . The hysteresis is defined as $\Delta V_{\text{hys}} = V_{\text{DP}}^{\text{forward}} - V_{\text{DP}}^{\text{reverse}}$ for the V_{TG} sweep. (d) Comparison of C_{Total} as a function of $V_{\text{TG}} - V_{\text{DP}}$ for the graphene FET devices fabricated by HP-PDA and AP-PDA.⁴ Solid circles are experimental data, while solid lines are curves fitted by $C_{\text{para}} = 0.10 \mu\text{Fcm}^{-2}$ for HP-PDA and $C_{\text{para}} = 0.19 \mu\text{Fcm}^{-2}$ for AP-PDA. (e) C_Q extracted based on the fitting in (d). The dotted line is the theoretical C_Q . The right vertical axis is converted to the DOS. n^* is $3.6 \times 10^{11} \text{ cm}^{-2}$ for both HP-PDA and AP-PDA.

Y_2O_3 topgate graphene devices shown in **Fig. 4(a)**. The Y_2O_3 insulator fabricated by HP-PDA is crystallized as a cubic phase (the inset in **Fig. 4(a)**); however, an amorphous region is also detected around the crystallized grain. On the other hand, the Y_2O_3 insulator fabricated by AP-PDA has very limited partial crystallization.²² The increase in the dielectric constant by HP-PDA is explained by the higher dielectric constant of crystalline Y_2O_3 . Interestingly, the formation of a two-dimensional hexagonal Y_2O_3 monolayer on graphene has been recently reported.²³ However, we did not observe a specific crystallographic relationship between Y_2O_3 and graphene. Moreover, electron energy loss spectroscopy (EELS) detected the NiO_x region on the Y_2O_3 insulator, which may have been formed by the annealing at 300 °C under the 0.1% O_2 gas flow after the topgate electrode deposition, as shown in **Fig. 4(b)**. This observation explains the apparently low k value of 5.4 for the HP-PDA Y_2O_3 insulator with a $C_{\text{Y}_2\text{O}_3} = 0.95 \text{ mFcm}^{-2}$ and a thickness of 5 nm. The topgate insulator in this study should be recognized as a gate stack of NiO_x and Y_2O_3 double layer.

Finally, we discuss the role of graphene as a diffusion barrier during HP-PDA. **Figure 4(c)** shows the capacitance as a function of the gate voltage for Au/ Y_2O_3 /n-Si MOS capacitors fabricated by AP-PDA

and HP-PDA. The considerable degradation of the capacitance for the accumulation side for HP-PDA indicates that the decrease in the k value for the Y_2O_3 insulator is due to the diffusion of Si into the Y_2O_3 , which has been reported previously.²⁴ On the other hand, the C_{total} for Y_2O_3 on graphene increases for HP-PDA, as shown in **Fig. 3(d)**. Si diffusion in Y_2O_3 is not detected within the resolution of the EELS measurements shown in **Fig. 4(b)**. Although the tail of the composition profile is generally $\sim 2 \text{ nm}$ in length due to the spatial extent of the electron beam, the lack of Si at the center of the Y_2O_3 profile and similar slopes for both the Y and O profiles support our premises. These results suggest that the increase in P_{O_2} by HP-PDA are totally spent on the improvement of the crystallinity and the reduction of defects such as oxygen vacancies, rather than on the diffusion of the other elements, because graphene is known to work as a diffusion barrier,²⁵⁻²⁷ as schematically explained in **Fig. 4(d)**. HP-PDA is applicable to other high- k materials on graphene, because the difference in ΔG° is very small for high- k materials. Moreover, this method may be extended to other layered materials with relatively high melting points.

HP-PDA is the robust method to drastically improve

Table 1 Summary of maximum E_F in the C_Q measurements

Insulator	Deposition method	Graphene	E_F [eV]	n [cm^{-2}]	Thickness [nm]	C_{ox} [μFcm^{-2}]	Ref.
Al_2O_3	ALD	ME*	0.3	$\sim 6.5 \times 10^{12}$	10	0.56	28
Al_2O_3	Depo. in O_2	ME	0.35	$\sim 10 \times 10^{12}$	10	0.47	2
Y_2O_3	Metal depo. & Air anneal	ME	0.4	$\sim 10 \times 10^{12}$	3.9	1.89	1
HO_2	ALD**	CVD	0.3	$\sim 6.5 \times 10^{12}$	4.4	1.98	29
h-BN	ME & Transfer	ME	0.26***	$\sim 5 \times 10^{12}$	27	0.15	30
Y_2O_3	Depo. in O_2 & HP-PDA	ME	0.52	$\sim 20 \times 10^{12}$	-	0.95	present
BMIM- PF_6	Ion gate	ME	0.22	$\sim 3.5 \times 10^{12}$	~ 0.3	~ 21	31
ABIM-TFSI	Ion gate	ME	0.82***	$\sim 50 \times 10^{12}$	-	-	32
Solid polymer	Ion gate	ME	1.17***	$\sim 100 \times 10^{12}$	-	~ 3.2	33

*"ME" indicates mechanical exfoliation of bulk graphite. **ALD HfO_2 is deposited on embedded metal and CVD graphene is transferred on HfO_2 . The device has inverted structure. *** E_F for these cases was calculated from the carrier density.

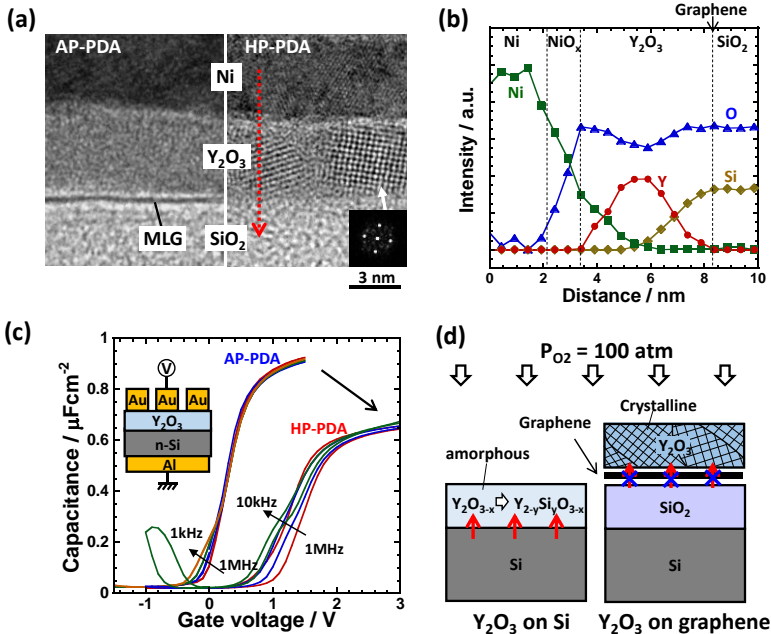


FIG. 4. (a) Cross-sectional TEM images for the graphene FET devices fabricated by HP-PDA and AP-PDA. The inset shows the Fourier transform of the Y_2O_3 grain marked by an arrow, confirming the cubic structure. (b) Intensity profiles as a function of distance along the dotted red line in (a), determined by the EELS measurements. It should be noted that the full-width at half-maximum for the Y profile is narrower than the thickness of Y_2O_3 determined from the TEM image because the detection sensitivity for the Y element is lower than for the other elements. (c) Bi-directional C - V characteristics for the Au/ Y_2O_3 /n-Si MOS capacitor fabricated by HP-PDA and AP-PDA at RT. (d) Schematics of the effect of HP-PDA for Y_2O_3 on Si (left) and Y_2O_3 on graphene/ SiO_2 /Si (right).

the electrical quality of high- k insulators without elevating the annealing temperature. The key to this process is that the increase in P_{O_2} by HP-PDA is totally spent on the improvement of crystallinity and the reduction of defects such as oxygen vacancies, rather than on the diffusion of other elements, because graphene works as a diffusion barrier. Using the high-quality Y_2O_3 insulator, we demonstrate the largest E_F (0.52 eV) reported to date in solid-state topgate insulators as well as the high transistor performance.

We are grateful to Covalent Materials for kindly providing the Kish graphite. K. N. acknowledges financial support from the JSPS through its ‘‘Funding Program for World-Leading Innovative R&D on Science and Technology (FIRST Program)’’ and from a Grant-in-Aid for Scientific Research on Innovative Areas and for Young scientists by the Ministry of Education, Culture, Sports, Science and Technology in Japan.

1. Z. Wang, H. Xu, Z. Zhang, S. Wnag, L. Ding, Q. Zeng, L. Yang, T. Pei, X. Liang, M. Gao, and L. -M. Peng, *Nano Lett.* **10**, 2024 (2010).
2. L. A. Ponomarenko, R. Yang, R. V. Gorbachev, P. Blake, A. S. Mayorov, K. S. Novoselov, M. I. Katsnelson, and A. K. Geim, *Phys. Rev. Lett.* **105**, 136801 (2010).
3. H. Miyazaki, K. Tsukagoshi, A. Kanda, M. Otani, and S. Okada, *Nano Lett.* **10**, 3888 (2010).
4. K. Nagashio, T. Nishimura, and A. Toriumi, *Appl. Phys. Lett.* **102**, 173507 (2013).
5. Z. H. Ni, H. M. Wang, J. Kasim, Y. H. Wu, and Z. X. Shen, *ACS Nano* **2**, 1033 (2008).
6. X. Wang, S. M. Tabakman, and H. Dai, *J. Am. Chem. Soc.* **130**, 8152 (2008).
7. J. M. P. Alaboson, Q. H. Wang, J. D. Eney, A. L. Lipson, M. J. Bedzyk, J. W. Elam, M. J. Pellin, and M. C. Hersam, *ACS Nano* **5**, 5223 (2011).
8. S. Jandhyala, G. Mordi, B. Lee, G. Lee, C. Floresca, P. -R. Cha, J. Ahn, R. M. Wallace, Y. J. Chabal, M. J. Kim, L. Colombo, K. Cho, and J. Kim, *ACS Nano* **6**, 2722 (2012).
9. B. Fallahazad, K. Lee, G. Lian, S. Kim, C. M. Corbet, D. A. Ferrer, L. Colombo, and E. Tutuc, *Appl. Phys. Lett.* **100**, 093112 (2012).
10. K. Kita, K. Kyuno, and A. Toriumi, *Appl. Phys. Lett.* **86**, 102906 (2005).
11. L. Liu, S. Ryu, R. M. Tomasik, E. Stolyarova, N. Jung, M. S. Hybertsen, M. L. Steigerwald, L. E. Brus, and G. W. Flynn, *Nano Lett.* **8**, 1965 (2008).
12. D. R. Gaskell, *Introduction to the metallurgical thermodynamics*, (2nd ed. McGraw-Hill, New York, 1981).
13. I. Barin, *Thermodynamical Data of Pure Substances, Part I&II*, (VCH Verlags Gesellschaft, Weinheim, 1993).
14. K. Watanabe, T. Taniguchi, and H. Kanda, *Nature Mater.* **3**, 404 (2004).
15. J. Robertson, *Rep. Prog. Phys.* **69**, 327 (2006).
16. C. R. Dean, A. F. Young, I. Meric, C. Lee, L. Wang, S. Sorgenfrei, K. Watanabe, T. Taniguchi, P. Kim, K. L. Shepard, and J. Hone, *Nature Nanotech.* **5**, 722 (2010).
17. See supplementary material at [http://].
18. T. Fang, A. Konar, H. Xing, and D. Jena, *Appl. Phys. Lett.* **91**, 092109 (2007).
19. K. Nagashio, T. Yamashita, T. Nishimura, K. Kita, and A. Toriumi, *J. Appl. Phys.* **110**, 024513 (2011).
20. S. Adam, E. H. Hwang, V. M. Galitski, and S. Das Sarma, *PNAS* **104**, 18392 (2007).
21. D. K. Schroder, *Semiconductor material and device characterization*, (Wiley interscience, New Jersey, 2006, p 490).
22. L. Wang, X. Chen, Y. Wang, Z. Wu, W. Li, Y. Han, M. Zhang, Y. He, C. Zhu, K. K. Fung, and N. Wang, *Nanocale*, **5**, 1116 (2013).
23. R. Addou, A. Dahal, and M. Batzill, *Nature Nanotechnol.* **8**, 41 (2013).
24. J. J. Chambers, and G. N. Parsons, *Appl. Phys. Lett.* **77**, 2385 (2000).
25. S. Chen, L. Brown, M. Levendorf, W. Cai, S. -Y. Ju, J. Edgeworth, X. Li, C. W. Magnuson, A. Velamakanni, R. D. Piner, J. Kang, J. Park, and R. S. Ruoff, *ACS Nano* **5**, 1321 (2011).
26. H. -Y. Kim, C. Lee, J. Kim, F. Ren, and S. J. Pearton, *J. Vac. Sci. Technol. B* **30**, 030602 (2012).
27. H. Tian, H. -Y. Chen, B. Gao, S. Yu, J. Liang, Y. Yang, D. Xie, J. Kang, T. -L. Ren, Y. Zhang, and H. -S. P. Wong, *Nano Lett.* **13**, 651 (2013).
28. Z. Chen, and J. Appenzeller, *IEDM Tech. Dig.* 509 (2008).
29. S. -J. Han, D. Reddy, G. D. Carpenter, A. D. Franklin, and K. A. Jenkins, *ACS Nano* **6**, 5220, (2012).
30. G. L. Yu, R. Jalil, B. Belle, A. S. Mayorov, P. Blake, F. Schedin, S. V. Morozov, L. A. Ponomarenko, F. Chiappini, S. Wiedmann, U. Zeitler, M. I. Katsnelson, A. K. Geim, K. S. Novoselov, and C. Elias, *PNAS*, **110**, 3282 (2013).
31. J. Xia, F. Chen, J. Li, and N. Tao, *Nature Nanotech.* **4**, 505 (2009).
32. J. Ye, M. F. Craciun, M. Koshino, S. Russo, S. Inoue, H. Yuan, H. Shimotani, A. F. Morpurgo, and Y. Iwasa, *PNAS* **108**, 13002 (2011).
33. D. K. Efetov, and P. Kim, *Phys. Rev. Lett.* **105**, 256805 (2010).